Vol. 33 (2002) *ACTA PHYSICA POLONICA B* No 12

# CP VIOLATION MEASUREMENTS AT *B* FACTORIES*

Henryk Pałka

H. Niewodniczański Institute of Nuclear Physics
Radzikowskiego 152, 31-342 Kraków, Poland

*(Received November 21, 2002)*

Recent results from KEK-B and PEP-II $B$ factories are reviewed with an emphasis on measurements of CP violating effects involving $B^0$ meson oscillations.

PACS numbers: 13.25.Hw, 12.15.Hh, 11.30.Er

## 1. Introduction

CP violation has been studied in the $K^0$ system for nearly forty years since its discovery in $K^0_{\rm L}$ decays. The measured strength of the CP violation ($\varepsilon$ and $\varepsilon^{'}$) can be accommodated in the Standard Model in a simple way [1]. Yet, the consistency of these results with the general scheme of charged weak interactions and CP violation in the Standard Model is non-trivial and further investigations must be pursued. The $B$ meson system, where the predicted effects are large, is particularly promising for quantitative tests of the Standard Model description of CP violation. For this purpose the new generation of $B$ factory experiments have been built and put into operation at KEK (Belle) and SLAC (BaBar).

These lectures overview the present experimental status of CP violation studies in the $B$ meson system. The content of the lectures is based on the Belle experiment data, the BaBar's results are also referred to. I start with a brief introduction to the Standard Model description of CP violation. In sections 2–4 I describe the experimental environment at $B$ factories: the properties of the $B$ mesons source, the colliders and the detectors. In the next sections two results concerning CP violation effects which involve $B^0$ oscillations are discussed. First, I overview the status of the primary milestone of $B$ factories: the measurement of the $\sin 2\phi_1$ (also known as $\sin 2\beta$) in $B^0 \to J/\psi K^0$ decays. Next, I describe the analysis of $B^0 \to \pi^+\pi^-$ decays, where direct CP violation might appear in a form of a time dependent effect.

* Presented at the XLII Cracow School of Theoretical Physics, Zakopane, Poland May 31–June 9, 2002.

## 2. CP violation in $B$ meson decays

In the Standard Model of electroweak interactions, CP violation is closely related to the Cabibbo–Kobayashi–Maskawa (CKM) matrix, connecting the electroweak eigenstates $(d', s', b')$ of the down, strange and bottom quarks with their mass eigenstates $(d, s, b)$ through the unitary transformation:

$$\begin{pmatrix} d' \\ s' \\ b' \end{pmatrix} = \begin{pmatrix} V_{ud} & V_{us} & V_{ub} \\ V_{cd} & V_{cs} & V_{cb} \\ V_{td} & V_{ts} & V_{tb} \end{pmatrix} \cdot \begin{pmatrix} d \\ s \\ b \end{pmatrix} \equiv \hat{V}_{\mathrm{CKM}} \cdot \begin{pmatrix} d \\ s \\ b \end{pmatrix} . \qquad (1)$$

The elements of the CKM matrix describe charged-current couplings.

### *2.1. Parametrisations of the CKM matrix*

For six quarks, three Euler-type angles and a single complex phase are needed to parametrize the CKM matrix. This complex phase is the single source of CP violation in the Standard Model, as was shown by Kobayashi and Maskawa in 1973 [1]. In one of possible parametrizations (the "standard parametrization" [2]), the three-generation CKM matrix takes the form

$$\begin{pmatrix} c_{12}c_{13} & s_{12}c_{13} & s_{13}e^{-i\delta_{13}} \\ -s_{12}c_{23} - c_{12}s_{23}s_{13}e^{i\delta_{13}} & c_{12}c_{23} - s_{12}s_{23}s_{13}e^{i\delta_{13}} & s_{23}c_{13} \\ s_{12}s_{23} - c_{12}c_{23}s_{13}e^{i\delta_{13}} & -c_{12}s_{23} - s_{12}c_{23}s_{13}e^{i\delta_{13}} & c_{23}c_{13} \end{pmatrix} , \qquad (2)$$

where $c_{ij} = \cos\theta_{ij}$ and $s_{ij} = \sin\theta_{ij}$.

The observed hierarchy of the strengths of the quark transitions mediated through charged-current interactions implies that

$$s_{12} = 0.22 \gg s_{23} = \mathcal{O}(10^{-2}) \gg s_{13} = \mathcal{O}(10^{-3}) . \qquad (3)$$

By introducing new parameters $\lambda$, $A$, $\rho$ and $\eta$ via relations

$$s_{12} \equiv \lambda = 0.22, \quad s_{23} \equiv A\lambda^2, \quad s_{13}e^{-i\delta} \equiv A\lambda^3(\rho - i\eta) , \qquad (4)$$

the standard parametrization (2) becomes:

$$\hat{V}_{\mathrm{CKM}} = \begin{pmatrix} 1 - \frac{1}{2}\lambda^2 & \lambda & A\lambda^3(\rho - i\,\eta) \\ -\lambda & 1 - \frac{1}{2}\lambda^2 & A\lambda^2 \\ A\lambda^3(1 - \rho - i\,\eta) & -A\lambda^2 & 1 \end{pmatrix} + \mathcal{O}(\lambda^4) . \qquad (5)$$

The phase convention is such, that all the CKM matrix elements are real except $V_{ub}$ and $V_{td}$. This approximation is called the "Wolfenstein parametrization" of the CKM matrix [3]. It corresponds to an expansion in powers of the small quantity $\lambda = 0.22$, and is useful for phenomenological analyses. The precision of the leading order terms is adequate to the current measurement errors, however the next-to-leading order terms in $\lambda$ will be needed soon with the data samples being accumulated at the $B$ factories.

### *2.2. The unitarity triangles of the CKM matrix*

The unitarity of the CKM matrix, $V_{\mathrm{CKM}}^{\dagger} \cdot V_{\mathrm{CKM}} = 1 = V_{\mathrm{CKM}} \cdot V_{\mathrm{CKM}}^{\dagger}$, leads to a set of twelve equations. Six of them represent normalisation relations and another six are orthogonality relations. The orthogonality relations can be represented as six triangles in the complex plane, all having the same area. In only two of them however, all three sides have comparable magnitudes $\mathcal{O}(\lambda^3)$. The orthogonality relations for the "non-squashed" triangles are given by

$$V_{ud}\, V_{ub}^{*} + V_{cd}\, V_{cb}^{*} + V_{td}\, V_{tb}^{*} \;=\; 0\,, \tag{6}$$

$$V_{ub}^{*}\, V_{tb} + V_{us}^{*}\, V_{ts} + V_{ud}^{*}\, V_{td} \;=\; 0\,. \tag{7}$$

The equation (6) results from the product of 1st and 3rd column and the equation (7) from the product of 1st and 3rd row of the CKM matrix. These two relations become identical in the Wolfenstein parametrization (at leading order in $\lambda$) yielding

$$(\rho + i\eta)A\lambda^3 + (-A\lambda^3) + (1 - \rho - i\eta)A\lambda^3 = 0\,. \tag{8}$$

The triangle in the $\rho$–$\eta$ plane corresponding to (8) is called "the" unitarity triangle of the CKM matrix. The relation (6) defines another form which is also commonly used to discuss measurements related to the unitarity triangle. The triangle in this form is shown in Fig. 1. It involves the two smallest elements of the CKM matrix, $V_{ub}$ and $V_{td}$. $V_{ub}$ is involved in $b \to u$ transitions such as in $B$ meson decays to charmless final states. $V_{td}$ appears in $b \to d$ transitions that can proceed via diagrams involving virtual top quarks, examples of which are the box diagrams describing the $B^0\bar{B}^0$ mixing. Because the lengths of the sides of the unitarity triangle are of the same order, the angles can be large, leading to potentially large CP-violating asymmetries from phases between CKM matrix elements.

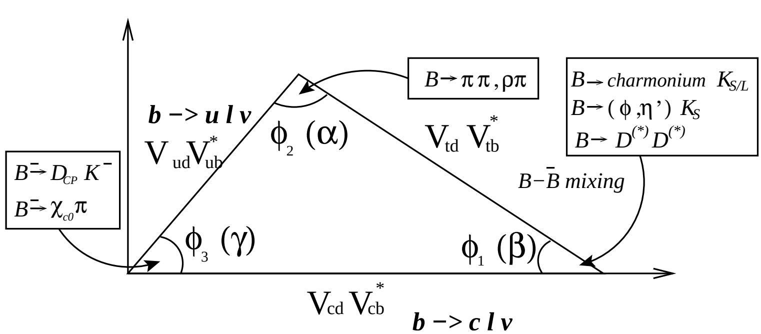


Fig. 1. The unitarity triangle and the processes to measure its elements.

The side of the unitarity triangle that is proportional to $V_{td}V_{tb}^*$ forms an angle $\phi_1(\beta)$[1] with the side proportional to $V_{cd}V_{cb}^*$ and an angle $\phi_2(\alpha)$ with the side proportional to $V_{ud}V_{ub}^*$. Experimental sensitivity to the angles $\phi_1$ and $\phi_2$ can therefore arise from interferences between the $B^0\bar{B}^0$ mixing amplitude (which involves $V_{td}$) and decay amplitudes that involve $V_{cb}$ and $V_{ub}$, respectively. The third angle, $\phi_3(\gamma)$, is the argument of $V_{ub}^*$.

The main aim of the $B$ factories experiments is to over-constrain the unitarity triangle by the measurements of its elements in many processes. Such multiple measurements will precisely constrain the position of the apex of the unitarity triangle and test a consistency of the Standard Model description of CP violation.

### *2.3. Flavour oscillations*

The ability of a few neutral mesons (recently also neutrinos) to change from their particle to their anti-particle state is a remarkable consequence of quantum mechanics and the structure of the weak interactions. If the physical particles are a mixture of states of well defined flavour, then these flavour eigenstates can be considered mixtures of the physical particles. The masses of these physical particles must slightly differ, so they develop a phase difference as they evolve in time. Therefore the physical particle content of a flavour eigenstate evolves with time: an initially pure flavour eigenstate develops a component of the opposite flavour. The mixing of flavour eigenstates to form the physical particles is then equivalent to the oscillations of flavour eigenstates into one another.

The light $B_{\mathrm{L}}$ and heavy $B_{\mathrm{H}}$ mass eigenstates of the neutral $B_d$ meson, made of $b$ and $d$ quarks, are given by[2]:

$$|B_{\mathrm{L}}\rangle = p\,|B^0\rangle + q\,|\bar{B}^0\rangle\,, \quad |B_{\mathrm{H}}\rangle = p\,|B^0\rangle - q\,|\bar{B}^0\rangle\,. \tag{9}$$

$B^0$ and $\bar{B}^0$ are the flavour eigenstates. They are related via CP transformation: $\mathrm{CP}\,|B^0\rangle = e^{2i\zeta_B}\,|\bar{B}^0\rangle$, where $\zeta_B$ is the arbitrary phase. The complex coefficients $p$ and $q$ are normalized ($|p|^2+|q|^2=1$). The phase of $q/p$ depends on phase conventions and is not an observable; only the modulus of this quantity, $|p/q|$, has a physical meaning.

The mass difference $\Delta m_{B_d}$ and width difference $\mathit{\Gamma}_{B_d}$ between the two mass eigenstates are defined as:

$$\Delta m_{B_d} \equiv m_{B_{\mathrm{H}}} - m_{B_{\mathrm{L}}}\,, \quad \Delta\mathit{\Gamma}_{B_d} \equiv \mathit{\Gamma}_{B_{\mathrm{H}}} - \mathit{\Gamma}_{B_{\mathrm{L}}}\,. \tag{10}$$

[1] The naming convention for angles in the triangle of Fig. 1 is the one used by Belle. The other widely used convention is also given in parenthesis.

[2] CPT invariance is assumed.

The two mesons are expected to have a negligible difference in lifetime, $\Delta\Gamma_{B_d}/\Gamma_{B_d} \sim 10^{-2}$ [4]. In particular, $\Delta\Gamma_{B_d}/\Gamma_{B_d} \ll x_d$, where $x_d \equiv \Delta m_{B_d}/\Gamma_{B_d} = 0.73 \pm 0.05$. Neglecting $\Delta\Gamma_{B_d}$, the time evolution of a state prepared initially (*i.e.* at time $t = 0$) in a pure $B^0$ or $\bar{B}^0$ state, can be written as:

$$\begin{aligned} \left|B^0_{phys}(t)\right\rangle &= e^{-imt} e^{-\frac{\Gamma t}{2}} \left[\cos\frac{\Delta m_{B_d} t}{2} |B^0\rangle + i\left(\frac{q}{p}\right) \sin\frac{\Delta m_{B_d} t}{2} |\bar{B}^0\rangle\right] , \\ \left|\bar{B}^0{}_{phys}(t)\right\rangle &= e^{-imt} e^{-\frac{\Gamma t}{2}} \left[\cos\frac{\Delta m_{B_d} t}{2} |\bar{B}^0\rangle + i\left(\frac{p}{q}\right) \sin\frac{\Delta m_{B_d} t}{2} |B^0\rangle\right] , \end{aligned} \tag{11}$$

where $m = \frac{1}{2}(m_{B_\mathrm{H}} + m_{B_\mathrm{L}})$ and $\Gamma = \frac{1}{2}(\Gamma_{B_\mathrm{H}} + \Gamma_{B_\mathrm{L}})$.

### *2.4. CP violation involving flavour oscillations*

The $B^0(\bar{B}^0)$ meson time-dependent decay rates to a specific final state $f$, which is accessible to both $B^0$ and $\bar{B}^0$, provide a rich ground for the observation of CP violating effects. Particularly interesting is the case where both transitions are of a comparable strength: $|T_f|^2 \approx |\overline{T}_f|^2$, with $T_f \equiv \langle f|H|B^0\rangle$ and $\overline{T}_f \equiv \langle f|H|\bar{B}^0\rangle$. This condition is met if the final state $f$ is a CP eigenstate, $f_{\mathrm{CP}}$.

Introducing the complex parameter $\lambda_f$: $\lambda_f \equiv \frac{q}{p}\frac{\overline{T}_f}{T_f}$ , the decay rates calculated from (11) are:

$$\rho_\pm(t) = \left\{\frac{1+|\lambda_{f_{\mathrm{CP}}}|^2}{2} \pm \frac{1-|\lambda_{f_{\mathrm{CP}}}|^2}{2}\cos\Delta m_{B_d} t \mp \mathrm{Im}(\lambda_{f_{\mathrm{CP}}})\sin\Delta m_{B_d} t\right\} e^{-\Gamma t} , \tag{12}$$

where

$$\begin{aligned} \rho_+(t) &\equiv |\langle f_{\mathrm{CP}}|H|B^0_{\mathrm{phys}}(t)\rangle|^2/|T_{f_{\mathrm{CP}}}|^2 \quad \text{and} \\ \rho_-(t) &\equiv |\langle f_{\mathrm{CP}}|H|\bar{B}^0{}_{\mathrm{phys}}(t)\rangle|^2/\,|\overline{T}_{f_{\mathrm{CP}}}|^2 . \end{aligned} \tag{13}$$

It can be seen from (12) that for $|\lambda_{f_{\mathrm{CP}}}| = 1$ and $\mathrm{Im}\,\lambda_{f_{\mathrm{CP}}} = 0$, the decay rates $\rho_+(t)$ and $\rho_-(t)$ are equal at any time, and thus no CP violation is present. In all other cases, for $\lambda_{f_{\mathrm{CP}}} \neq \pm 1$, the rates differ and time dependent CP violating effects can be observed. The observable is the time-dependent CP asymmetry:

$$\mathcal{A}_{\mathrm{CP}}(t) \equiv \frac{\Gamma(|\bar{B}^0{}_{\mathrm{phys}}(t)\rangle \to f_{\mathrm{CP}}) - \Gamma(|B^0_{\mathrm{phys}}(t)\rangle \to f_{\mathrm{CP}})}{\Gamma(|\bar{B}^0{}_{\mathrm{phys}}(t)\rangle \to f_{\mathrm{CP}}) + \Gamma(|B^0_{\mathrm{phys}}(t)\rangle \to f_{\mathrm{CP}})} . \tag{14}$$

It can be written as:

$$\mathcal{A}_{\mathrm{CP}}(t) = S_{f_{\mathrm{CP}}} \cdot \sin\Delta m_{B_d} t + A_{f_{\mathrm{CP}}} \cdot \cos\Delta m_{B_d} t , \tag{15}$$

where the coefficients of the sine and cosine terms are:

$$S_{f_{\rm CP}} = \frac{2\,{\rm Im}\lambda_{f_{\rm CP}}}{|\lambda_{f_{\rm CP}}|^2+1} \quad \text{and} \quad A_{f_{\rm CP}} = \frac{|\lambda_{f_{\rm CP}}|^2-1}{|\lambda_{f_{\rm CP}}|^2+1}\,. \tag{16}$$

CP violation arising from the weak phase difference between $q/p$ and $\frac{\overline{T}_{f_{\rm CP}}}{T_{f_{\rm CP}}}$ ($\Longrightarrow |\lambda_{f_{\rm CP}}| = 1, {\rm Im}\,\lambda_{f_{\rm CP}} \neq 0$), results in a non-vanishing sine term. In terms of flavour eigenstates, this CP violation effect is due to an interference between the decay of a $B^0$ meson with and without mixing.

In the case of the decay process involving a single weak phase $\phi_{\rm D}$, one obtains

$$\frac{\overline{T}_{f_{\rm CP}}}{T_{f_{\rm CP}}} = \xi_{f_{\rm CP}} e^{2i\phi_{\rm D}} e^{-2i\zeta_B}\,, \tag{17}$$

where $\xi_{f_{\rm CP}} = \pm 1$ is the CP parity of the final state $f_{\rm CP}$. It follows that:

$$\begin{aligned} \lambda_{f_{\rm CP}} &= \xi_{f_{\rm CP}} e^{2i(\phi_{\rm D}+\phi_{\rm M})}\,, \\ S_{f_{\rm CP}} &= {\rm Im}\lambda_{f_{\rm CP}} = \xi_{f_{\rm CP}} \sin 2(\phi_{\rm D}+\phi_{\rm M})\,, \\ A_{f_{\rm CP}} &= 0\,, \end{aligned} \tag{18}$$

where the phase $\phi_{\rm M} = \arg(V_{td}V_{tb}^*) \sim -\phi_1 (\equiv -\beta)$ results from CKM factors involved in the box diagrams describing the dispersive part of the $B^0 \to \bar{B}^0$ mixing amplitude. Using the usual phase convention, by which the ratio of amplitudes becomes real ($\phi_{\rm D} = 0$), the asymmetry becomes:

$$\mathcal{A}_{\rm CP}(t) = -\xi_{f_{\rm CP}} \sin 2\phi_1 \sin \Delta m_{B_d} t\,. \tag{19}$$

Note that the asymmetry vanishes in the time-integrated rate, therefore time dependent measurement is indispensable to observe the CP violating effect.

A theoretically clean way [5] of measuring $\sin 2\phi_1$ is provided by the "gold-plated" $J/\psi K^0_{S,L}$ decay modes ($\xi_{J/\psi K^0_{\rm S}} = -1, \xi_{J/\psi K^0_{\rm L}} = 1$). Their branching fractions are relatively high ($\sim 10^{-4}$) and experimental signatures are distinct. The decays proceed via the tree level quark diagram $b \to c\bar{c}s$ which involves the $V_{cs}^* V_{cb}$ product. A possible contribution from the penguin diagram $b \to sg^* \to sc\bar{c}$ is small and involves the same weak phase as the three diagram. Thus, direct CP violation is ruled out in these modes, with negligible theoretical uncertainty.

The cosine term in (15) is non-zero only when $|\frac{\overline{T}_{f_{\rm CP}}}{T_{f_{\rm CP}}}| \neq 1 \Longrightarrow |\lambda_{f_{\rm CP}}| \neq 1$. It signals the presence of CP violation in the decay (direct CP violation). Note that unlike the mixing induced CP violation, the direct CP violation cosine term in (15) does not time integrate to zero.

$B^0 \to \pi^-\pi^+$ is the promising decay mode to observe CP violation effect related to the cosine term. The amplitude for this decay mode can receive a contribution from a tree diagram $b \to u\bar{u}d$ as well as a Cabibbo suppressed gluonic penguin diagram $b \to dg^* \to du\bar{u}$. Recent measurements suggest that the penguin contribution is not negligible. A weak phase of the penguin contribution is different from the phase of the larger tree amplitude, and very likely their strong phases differ too. The presence of the extra contribution modifies also the mixing induced asymmetry term $S_{f_{\rm CP}}$, therefore its measurement will yield some $\sin 2\phi_2^{\rm eff}$.

## 3. *B* factories and detectors

Although CP violation effects in the $B$ meson system are larger than for $K$ mesons, their observation remained a significant experimental challenge. The challenge lies in the fact that $B$ mesons decay much more quickly than $K$ mesons. Therefore time dependent CP measurements for $B$ mesons involve an observation of flight distances of fractions of a millimetre, compared to meters for kaons. Furthermore, the decay rates to experimentally accessible CP eigenstates are very much smaller for $B$ mesons: $\mathcal{O}(10^{-4})$, contrary to the large $\mathcal{O}(1)$ branching fractions of kaons. Therefore, the prerequisite of the CP violation observation is a high luminosity source of $B$ mesons produced with a boost to dilate their decay distances. Such sources have been nicknamed "$B$ factories", for their ability to produce $B$ meson samples exceeding by order of magnitude data samples available at a conventional collider like CESR.

### *3.1. The concept of an asymmetric beam energy B factory*

The $\Upsilon(4S)$ resonance that is formed in $e^+e^-$ annihilation at $\sqrt{s} \approx$ 10.58 GeV is the cleanest source of $B$ mesons. The resonance is the lightest $b\bar{b}$ bound state with quantum numbers $J^{\rm PC} = 1^{--}$, the first one occurring above $B$ meson pair production threshold. The cross-section for the resonance formation is approximately 1 nb, and it competes with $\sim 3$ times stronger QED continuum production $e^+e^- \to q\bar{q}$ (where $q = u, d, s, c$). This modest continuum background can be effectively suppressed thanks to distinct topological characteristics of $B\bar{B}$ events.

The $\Upsilon(4S)$ decays exclusively into $B^+B^-$ and $B^0\bar{B}^0$ final states[3], with approximately equal rates. Due to the intrinsic spin of the $\Upsilon(4S)$ the produced $B^0\bar{B}^0$ pairs are in a coherent $L = 1$ state. Each neutral meson of the pair evolves according to the time evolution of a single $B^0$ meson given by equations (11). The two mesons evolve coherently (they are entangled) and

[3] Experimentally, this statement has a 4% accuracy: $BF(\Upsilon(4S) \to {\rm non}{-}B\bar{B}) \leq 4\%$ [2].

the correlation between them holds at any time after production until one of them decays. If the first meson decays into a flavour specific final state (or into a CP eigenstate), the other meson in the pair, at the same instant, must have the opposite flavour (the opposite CP eigenvalue).

The mean lifetime of $B$ mesons amounts to $\sim 1.5\,\mathrm{ps}$. Therefore, the mesons produced from the $\Upsilon(4S)$ decay, having momenta $\sim 330\,\mathrm{MeV}$, travel on average only $\sim 30\,\mu\mathrm{m}$ before they decay. Such flight distances are too small to be measured with currently available detector technologies, making time-dependent studies of the decay rates asymmetries impossible. These measurements were not possible at the CESR symmetric energy storage ring at Cornell which operated for nearly two decades.

To resolve this problem, an asymmetric beam energy $e^+e^-$ collider operating at the $\Upsilon(4S)$ was proposed [6] in the late 1980s. In such an arrangement, the $\Upsilon(4S)$ is produced with a boost in the laboratory frame and the $B$ mesons emerging from the resonance travel measurable distances along the boost axis before they decay.

### *3.2. B factory accelerators*

Two asymmetric beam energy $e^+e^-$ colliders have been built and commissioned in late 1998 to accomplish a program of CP violation studies in the $B$ system: PEPII at SLAC in the United States and KEKB at KEK in Japan. The layout of KEK-B, situated in the tunnel previously hosting TRISTAN collider, is shown in Fig. 2. PEPII collider also partially reuses facilities of PEP machine.

Design parameters of both colliders are summarised in Table I. The asymmetric $B$ factories use double storage rings and very large numbers of bunches to obtain high luminosity. The currents of the individual bunches are similar to that achieved at conventional storage rings such as CESR. Because of the high bunch density, the operation of complex feedback systems is needed to avoid beam instabilities due to coupling between bunches.

The beam energy asymmetry is slightly larger for PEP-II than for KEK-B, resulting in the center-of-mass boosts $\beta\gamma = 0.56$ and $\beta\gamma = 0.45$, respectively.

KEK-B employs the beam crossing angle scheme to minimise parasitic collisions between incoming and outgoing bunches. The crossing angle of KEK-B is 22mr. Beam collisions at such large angle have never been operated before. KEK-B continues development of special RF cavities (crab cavities) to rotate the bunches before crossing and collide them head on at the interaction point. The use of crab cavities will result in an additional gain in luminosity, while preserving all benefits of the crossing angle collisions.

PEP-II uses magnetic separation to suppress the effect of parasitic collisions. The use of strong magnets close to the interaction region results in

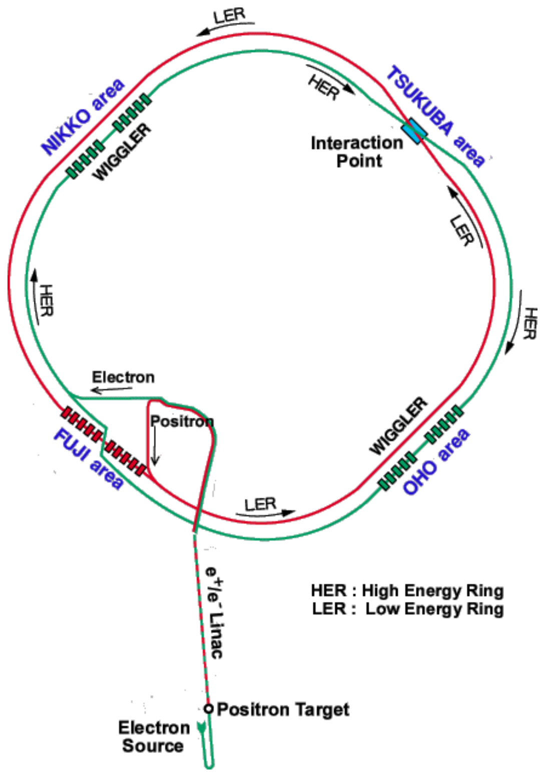


Fig. 2. Layout of KEK-B accelerator.

somewhat larger beam backgrounds, compared to the crossing angle scheme. It also imposes tighter constraints on the construction of the detector layers closest to the interaction region.

The performance achieved by both $B$ factories since the startup of physics runs in 1999 is quite remarkable. A comparison of integrated luminosities logged by each experiment at KEK-B and PEP-II is shown in Fig. 3.

By the summer of 2002, both $B$ factories delivered similar integrated luminosities and each experiment accumulated data sample corresponding to over 80 million $B\bar{B}$ pairs. The peak luminosity for PEP-II was $4.5 \times 10^{33}/\mathrm{cm}^2/\mathrm{sec}$ while KEK-B had achieved $7.4 \times 10^{33}/\mathrm{cm}^2/\mathrm{sec}$. The beam currents of KEK-B are still below the design values and the recent KEK-B instantaneous luminosities (the slope of the curve in Fig. 3) bodes well for upcoming data-taking.

TABLE I

Design parameters of $B$-factory accelerators.

| | | KEK-B | | PEP-II | |
|---|---|---|---|---|---|
| | | LER | HER | LER | HER |
| Energy | $E$(GeV) | 3.5 | 8.0 | 3.1 | 9.0 |
| $\beta\gamma(\Upsilon(4S))$ | | 0.45 | | 0.56 | |
| Luminosity | $L(\mathrm{cm}^{-2}\mathrm{s}^{-1})$ | $1 \times 10^{34}$ | | $3 \times 10^{33}$ | |
| Collision mode | | $\pm 11mr$ (crab) | | Head-on | |
| Circumference | $C$(m) | 3018 | | 2199 | |
| Beta function | $\beta_x^*/\beta_y^*$(cm) | 100/1 | 100/1 | 37.5/1.5 | 75/3 |
| Tune shift | $\xi_x/\xi_y$ | 0.05/0.05 | | 0.03/0.03 | |
| Emittance | $\varepsilon_x/\varepsilon_y$(nm) | 19/0.19 | 19/0.19 | 64/2.6 | 48.2/1.9 |
| Energy spread | $\sigma_E/E(10^{-4})$ | 7.7 | 7.2 | 9.5 | 6.1 |
| Total current | $I$(A) | 2.6 | 1.1 | 2.14 | 0.98 |
| No. of bunches | $N_{\mathrm{B}}$ | 5120 | | 1658 | |
| Bunch spacing | $S_{\mathrm{B}}$(m) | 0.6 | | 1.26 | |
| RF frequency | $f_{\mathrm{RF}}$(MHz) | 508 | | 476 | |
| RF voltage | $V_c$(MV) | 22 | 48 | 9.5 | 18.5 |
| Cavity type | | ARES | SC | 1-cell normal | |
| No. of cavities | | 28 | 60 | 10 | 20 |

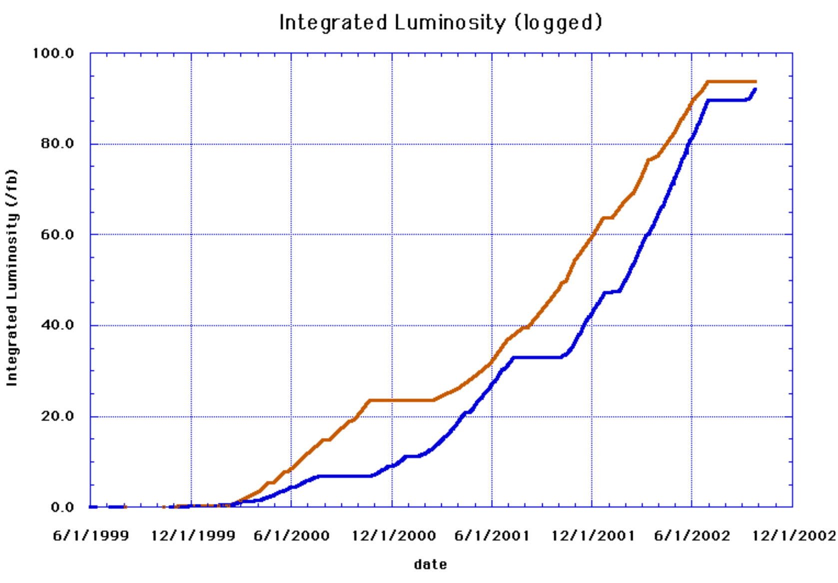


Fig. 3. The rate of integrated luminosity logged by the Belle experiment at KEK-B (lower line) and the BaBar at PEPII.

### *3.3. Detectors*

The most challenging requirement, for the $B$ factory detector is the detection of decay vertices of short lived particles. To deal with this requirement double-sided silicon strip detectors are employed. This technique in $e^+e^-$ environment has been mastered in experiments at LEP. However, its use was by no means straightforward in rather harsh radiation conditions and low momentum tracking of a $B$ factory experiment. The other difficult requirement for the $B$ factory detector is the efficient separation of kaons from pions over wide momentum range. This is particularly important at high momenta to be able to distinguish $\bar{B}^0 \to \pi^+\pi^-$ from a stronger decay $\bar{B}^0 \to K^-\pi^+$.

The concepts of the two detectors are similar. A comparison of their main components is shown in Table II and a schematic view of the Belle detector is shown in Fig. 4.

TABLE II

A comparison of main components of $B$ factory detectors: BaBar [7] and Belle [8].

| | BaBar | Belle |
|---|---|---|
| SVD | 5 layers | 3 layers |
| $r$ (cm) | 3.2 – 14.4 | 2 – 5.8 |
| CDC | 40 layers | 50 layers |
| $r$ (cm) | 24 – 80 | 9 – 86 |
| PID | DIRC+$dE/dx$ | Aerogel/TOF+$dE/dx$ |
| EM Calorimeter | CsI(Tl) | CsI(Tl) |
| Magnet | 1.5 T | 1.5 T |
| $K_{\mathrm{L}}/\mu$ | RPC<br>Linseed Oil | RPC<br>Glass |

Going outwards from the collision point in Belle, charged tracks from $B$ meson decay are measured in a three layer silicon vertex tracker (SVD) with a precision of $55\,\mu$m at a momentum of 1 GeV which results in about $100\,\mu$m precision in $z$ direction on the $B$ decay vertices. They next pass through a drift chamber (CDC) filled with a Helium based gas to minimise multiple scattering and effects of synchrotron radiation backgrounds. The chamber measures track momentum $p$ with a precision of $\sigma_p/p = (0.2\,p \oplus 0.3)\%$ providing excellent invariant mass resolutions. This is followed by an Cesium-Iodide crystal calorimeter, located inside the coil of the magnet, that has better than 2% energy resolution for 1 GeV photons.

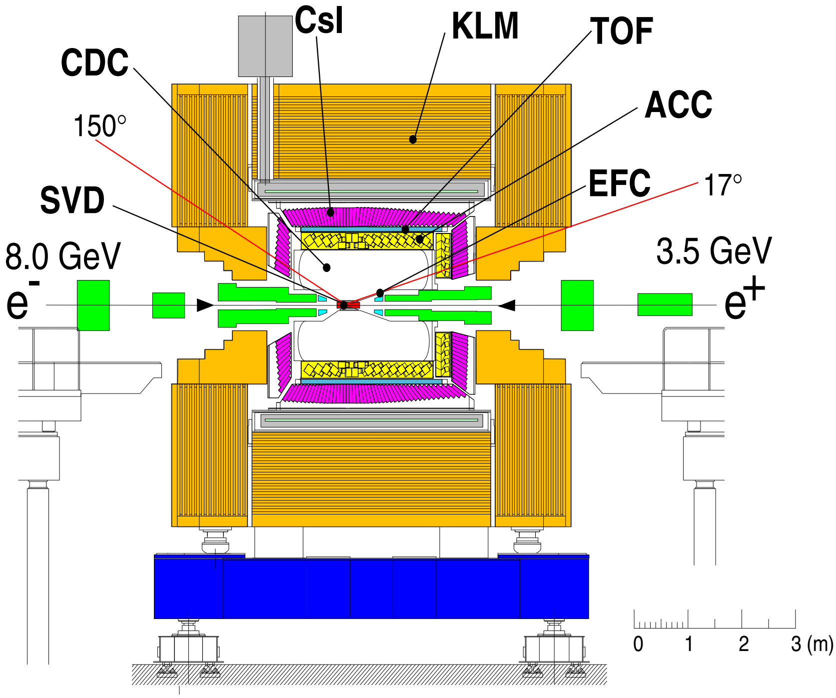


Fig. 4. A cross-section of the Belle detector.

Different approaches for high momentum particle identification have been implemented in Belle and BaBar. At Belle aerogel Cerenkov radiators (PID) are used. Aerogel blocks are readout by high gain fine-mesh photomultipliers which can operate in a 1.5 Tesla magnetic field. Since the threshold for the aerogel is around 1.5 GeV, $K/\pi$ separation below this momentum is carried out using high precision time-of-flight scintillators (TOF) with time resolution of 95 ps. The aerogel and TOF counter measurements are complemented by $dE/dx$ measurements in the CDC. The $dE/dx$ system provides $K/\pi$ separation in the ionisation loss relativistic rise region around 2.5 GeV and below 0.7 GeV. For high momentum kaons, an efficiency of 88% with a misidentification probability of 9% has been achieved. At BaBar a differential imaging ring Cerenkov (DIRC) detector is used. Cerenkov light is produced in quartz bars and then transmitted by internal reflection outside of the detector through a water tank to a large array of phototubes where the ring is imaged. The detector provides particle identification over the full momentum range for particles that are energetic enough to reach it. Additional particle identification is provided by $dE/dx$ measurements from the drift chamber and from the 5-layer SVD.

The last layer of the spectrometer, located behind the superconductive solenoid coil, consists of a $K^0_{\rm L}$ and muon detection system (KLM) that identifies muons with less than 2% fake rate above 1 GeV. Acting as a hadron absorber it also detects $K^0_{\rm L}$ showers with an angular resolution of few degrees.

## 4. The measurement of $\sin 2\phi_1$

The measurement of a CP violating phase in $B^0$ flavour oscillations requires three steps sketched in Fig. 5. First, a sample of $B^0 \to f_{\rm CP}$ decays into CP eigenstates has to be fully reconstructed. Secondly, the flavour of the $B^0 \to f_{\rm tag}$ meson accompanying the partner decayed to a CP eigenstate must be tagged. Finally, the decay vertices of the two $B^0$ mesons must be identified and their space coordinates measured, to obtain lifetimes difference $\Delta t$. These ingredients are briefly discussed in the following sections.

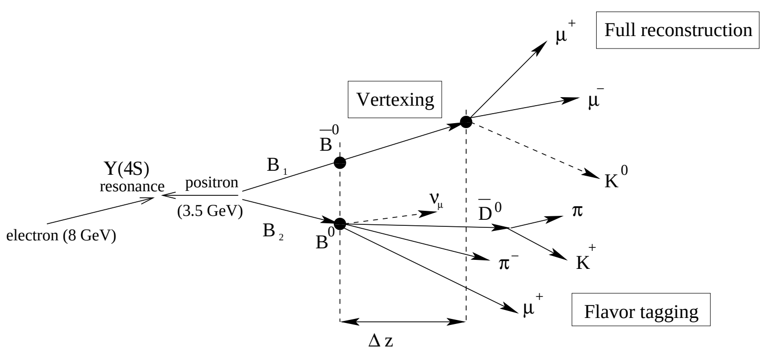


Fig. 5. An illustration of ingredients needed for a measurement of CP violation in $B^0$ oscillations.

### *4.1. CP eigenstate event samples*

Belle reconstructs about 3300 $B^0 \to (c\bar{c})K$ candidates, where $(c\bar{c})$ stands for $J/\psi\,, \psi(2S)\,, \chi_{c1}$ and $\eta_c$, from a sample of $78\,{\rm fb}^{-1}$ of data taken at the $\Upsilon(4S)$ resonance till summer 2002. These are summarised in Table III. The unstable particles in the final state are reconstructed in the decay modes which are listed in parentheses in Table III.

$B \to f_{\rm CP}$ decays are identified, except for $B \to J/\psi K^0_{\rm L}$, using the energy difference $\Delta E \equiv E_B - E_{\rm beam}$ and the beam-energy constrained mass $m_{\rm bc} \equiv \sqrt{(E_{\rm beam})^2 - (p_B)^2}$, where $E_{\rm beam}$ is the beam energy in the initial collision center-of-mass system (cms; $\equiv \Upsilon(4S)$ rest frame), and $E_B$ and $p_B$ are the cms energy and momentum of the reconstructed $B$ candidate.

TABLE III

Summary of $B^0 \to f_{\rm CP}$ candidates. $\xi_{f_{\rm CP}}$: CP eigenvalue; $N_{\rm rec}$: number of identified decay candidates $N_{\rm ev}$: number of events with flavour tagging and vertex reconstruction information used for the $\sin 2\phi_1$ determination.

| Mode | $\xi_{f_{\rm CP}}$ | $N_{\rm rec}$ | $N_{\rm ev}$ | Purity (%) |
|---|---|---|---|---|
| $J/\psi(\ell^+\ell^-)K^0_{\rm S}(\pi^+\pi^-)$ | $-1$ | 1285 | 1116 | $97.6 \pm 0.1$ |
| $J/\psi(\ell^+\ell^-)K^0_{\rm S}(\pi^0\pi^0)$ | $-1$ | 188 | 162 | $82 \pm 2$ |
| $\psi(2S)(\ell^+\ell^-)K^0_{\rm S}(\pi^+\pi^-)$ | $-1$ | 91 | 76 | $96 \pm 1$ |
| $\psi(2S)(J/\psi\pi^+\pi^-)K^0_{\rm S}(\pi^+\pi^-)$ | $-1$ | 112 | 96 | $91 \pm 1$ |
| $\chi_{c1}(J/\psi\gamma)K^0_{\rm S}(\pi^+\pi^-)$ | $-1$ | 77 | 67 | $96 \pm 1$ |
| $\eta_c(K^0_{\rm S}K^-\pi^+)K^0_{\rm S}(\pi^+\pi^-)$ | $-1$ | 72 | 63 | $65 \pm 4$ |
| $\eta_c(K^+K^-\pi^0)K^0_{\rm S}(\pi^+\pi^-)$ | $-1$ | 49 | 44 | $72 \pm 4$ |
| $\eta_c(p\overline{p})K^0_{\rm S}(\pi^+\pi^-)$ | $-1$ | 21 | 15 | $94 \pm 2$ |
| All with $\xi_{f_{\rm CP}} = -1$ | $-1$ | 1895 | 1639 | $93.6 \pm 0.3$ |
| $J/\psi(\ell^+\ell^-)K^{*0}(K^0_{\rm S}\pi^0)$ | $+1(81\%)$ | 101 | 89 | $92 \pm 1$ |
| $J/\psi(\ell^+\ell^-)K^0_{\rm L}$ | $+1$ | 1330 | 1230 | $63 \pm 4$ |
| All | | 3326 | 2958 | $81 \pm 1$ |

Majority of the reconstructed candidates decay to CP odd eigenstates, and the highest purity "golden mode" $J/\psi K^0_{\rm S}$ constitutes about one third of the total sample. We also use $B^0 \to J/\psi K^{*0}$ decays where $K^{*0} \to K^0_{\rm S}\pi^0$. Here the final state is a mixture of even and odd CP eigenstates, depending on the relative orbital angular momentum of the $J/\psi$ and $K^{*0}$. We find that the final state is primarily CP even; the $\xi_{f_{\rm CP}} = -1$ fraction is $0.19 \pm 0.02({\rm stat}) \pm 0.03({\rm syst})$ [10]. Figure 6 shows the $m_{\rm bc}$ distributions of the selected $B^0$ candidates except for $B^0 \to J/\psi K^0_{\rm L}$, that have $\Delta E$ values in the signal region.

Finally, candidate $B^0 \to J/\psi K^0_{\rm L}$ decays are selected by requiring ECL and/or KLM hit patterns that are consistent with the presence of a shower induced by a $K^0_{\rm L}$ meson. While these detectors can not measure the energy of the hadronic shower induced by a $K^0_{\rm L}$ precisely enough, they measure the direction of such a shower with a few degrees accuracy. With the hypothesis of a $B^0 \to J/\psi K^0_{\rm L}$ decay, and having measured the $K^0_{\rm L}$ direction, the magnitude of the $K^0_{\rm L}$ momentum can be inferred. Figure 7 shows the distribution of $B$ momenta in the rest frame of $\Upsilon(4S)$, calculated with the $B^0 \to J/\psi K^0_{\rm L}$ two-body decay hypothesis. The signal candidates peak near $p_B \approx 0.3$ GeV, while the three identified categories of backgrounds generate a flatter distribution. The histograms in Fig. 7 are the results of a fit to the

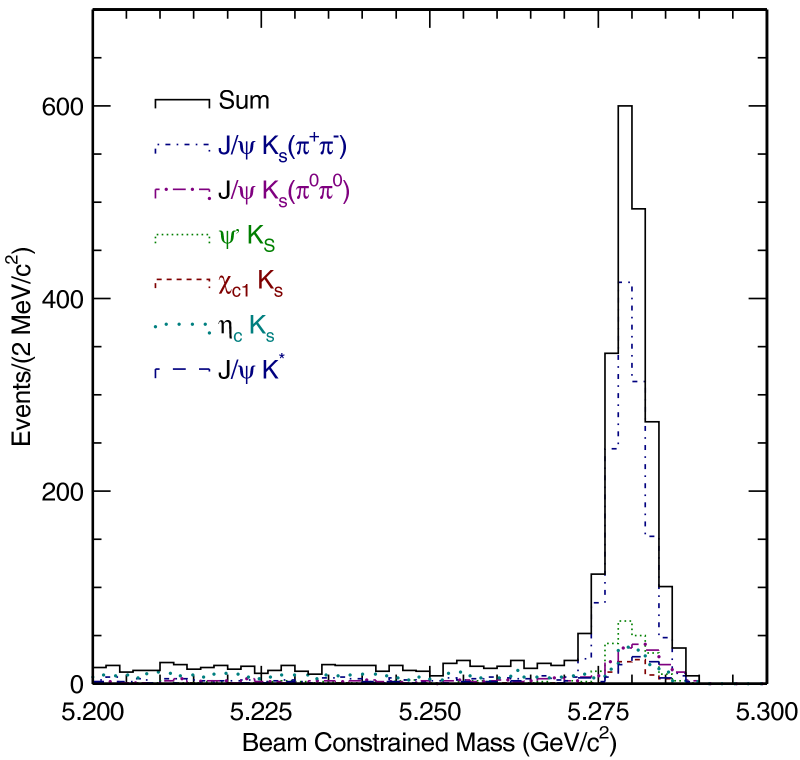


Fig. 6. The beam-energy constrained mass distribution for all $B^0$ decay candidates other than $B^0 \to J/\psi K^0_{\rm L}$.

signal and background distributions. There are 1330 signal candidates in the $0.20 \le p_B \le 0.45$ GeV signal region and the fit indicates a signal purity of 63%. A fraction of the background under the $p_B$ peak is due to other $B$ meson decays. The CP asymmetry of this background has been studied and the effect has been included in a systematic error on the measurement. Although the reconstruction of a good purity sample of CP even eigenstates $J/\psi K^0_{\rm L}$ is an experimental challenge, the measurement of its sign reversed, as compared to $J/\psi K^0_{\rm S}$, time-dependent asymmetry provides a crucial test of the experimental method.

More detailed description of the reconstruction and selection criteria for all $f_{\rm CP}$ final states used in the measurement can be found in Ref. [11].

The event yields in BaBar from the $\sim 80\,{\rm fb}^{-1}$ data sample [12] are similar. They select a total of 2640 events with the purity of 78% for the CP asymmetry analysis.

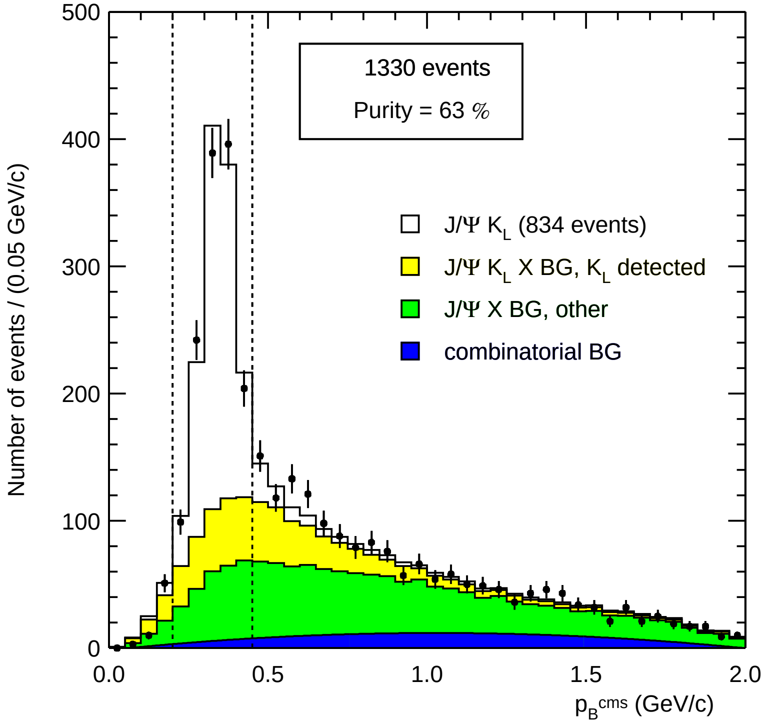


Fig. 7. The $p_B$ distribution for $B^0 \to J/\psi K^0_{\rm L}$ candidates with the results of the fit.

### *4.2. Flavour tagging*

Identification of the flavour of the $B$ meson accompanying the CP eigenstate is the second step of the analysis. Since only a small fraction of $B$ decays ($\mathcal{O}(10^{-3})$) could be reconstructed in exclusive channels we do this, for the sake of efficiency, without fully reconstructing the decay. For example, high momentum leptons in a partially reconstructed final state are indicative of a direct semi-leptonic $B$ decay and the charge of the lepton is a direct indication of the flavour of $B$. Lower momentum leptons from cascade semileptonic decays $b \to c \to l^-$ also give the flavour indication by the opposite correlation between the lepton charge and $B$ meson flavour. Similarly: kaons, charged slow pions from $D^* \to D^0\pi^+$ decays, and energetic pions from two-body $B$ decay (*e.g.* $\bar{B}^0 \to D^{*+}\pi^+$) can be used to identify the flavour of the accompanying $B$ meson. Such information is combined in a set of look-up tables shown in Fig. 8. The look-up tables classify flavour information according to the sign of the $b$ quark charge, $q = +1$ for $B^0$; $q = -1$ for $\bar{B}^0$, and the quality (reliability) of the tagging information, $0 \leq r \leq 1.0$. Here $r = 0$ corresponds to no flavour discrimination

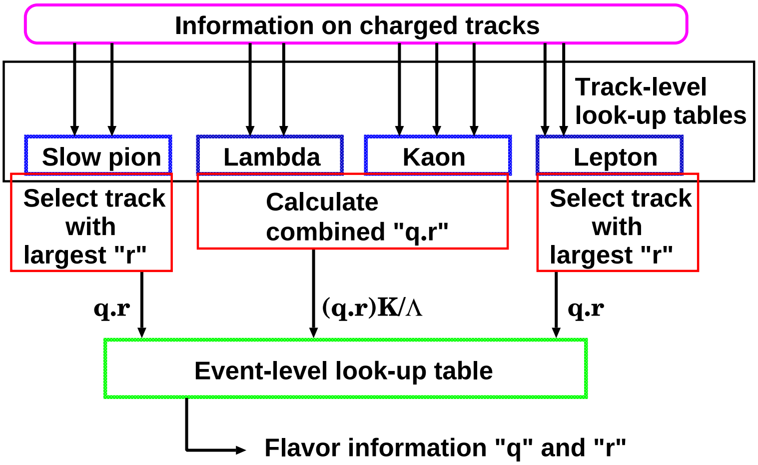


Fig. 8. A block diagram of the $B^0$ tagging algorithm. A set of look-up tables, based on MC simulation, is used to identify and quantify the flavour of the $B^0$ accompanying the $B^0 \to f_{\rm CP}$ decay.

and $r = 1$ gives an unambiguous flavour assignment. The look-up table information, $q$ and $r$, is extracted from a Monte Carlo simulation. It is used however only to sort data into six intervals of $r$, according to estimated flavour purity. The tagging algorithm is calibrated on the control data samples and the wrong-tag probabilities in each tagging reliability interval, $w_l$ $(l = 1, 6)$, that are used in the final CP fit are determined directly from data. Samples of $B^0$ decays to exclusively reconstructed self-tagging channels are used to obtain $w_l$ by measuring time-dependent $B^0$-$\overline{B^0}$ flavour oscillation. For example, we apply our tagging algorithm to reconstructed $B^0 \to D^- l^+ \nu_l$ events, for which the flavour of the $B$ is known from the charge of the lepton, to classify the tagging information on the accompanying $B$ meson into six ranges of $r$. The result is shown in Fig. 9 in terms of the time-dependent asymmetry between unmixed and mixed $B^0$ pairs. The asymmetry is $(N_{\rm of} - N_{\rm sf})/(N_{\rm of} + N_{\rm sf}) = (1 - 2w_l)\cos(\Delta m_d \Delta t)$, where $N_{\rm of}$ and $N_{\rm sf}$ are numbers of opposite and same flavour events, $\Delta t$ is the time difference measured from the distance $\Delta z$ between decay vertices and $\Delta m_d$ is the mixing parameter measured in dedicated analyses. With this definition, the decrease of the oscillation amplitude at $\Delta t = 0$ from a value of one (no mixing) measures the wrong flavour tag probability $w_l$. For no flavour discrimination: $w_l = 0.5$ and the oscillation pattern cannot be observed (the amplitude is zero); for a perfect flavour tag: $w_l = 0$, and the amplitude is maximal. As it can be seen from Fig. 9, for the highest flavour tag quality events $(0.875 \le r \le 1)$ the amplitude almost reaches the ideal value of 1; in this category the wrong flavour tag probability is $w_l = 0.020 \pm 0.006$. On the opposite end, for the least reliable flavour tag category ($0 \leq r \leq 0.25$) our ability to tag correctly the $B$ flavour is very limited: $w_l = 0.458 \pm 0.006$. We use these measured tag probabilities to weight CP eigenstate events when extracting time-dependent CP asymmetries.

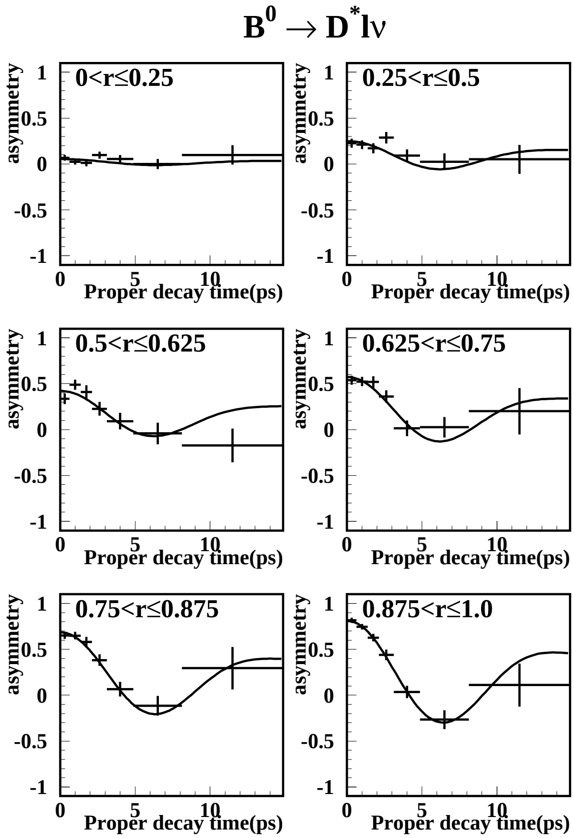


Fig. 9. $B^0$–$\bar{B}^0$ oscillation measurement in self-tagged $B^0 \to D^- l^+ \nu_l$ sample, used to determine wrong flavour tag probability.

This algorithm gives tagging information for 99.5% of the reconstructed CP eigenstate events. While some of the events have tags of low reliability, an overall tagging efficiency is $28.8 \pm 0.6\%$, corresponding to almost 1/3 of our $B$ sample being perfectly tagged.

BaBar's flavour tagging technique differs from our in details [12]. They obtain a similar tagging performance, with overall efficiency of $28.1 \pm 0.7\%$.

### *4.3. B meson decay vertex measurement*

In a $B$ factory experiment one lifetime of the $B^0$ meson corresponds to a decay distance of the order of $200\,\mu$m along the boost direction ($z$) and a full $B^0 \to \bar{B}^0$ mixing period is $2\pi/\Delta m_{B_d} \approx 1600\,\mu$m. The maximum of the time-dependent CP asymmetry (19) occurs at around a quarter period $400\,\mu$m, where the probabilities of mixed and unmixed $B^0$ states are equal. The Belle's silicon vertex detector measures the position of the decay vertex along the boost direction ($z$) with a precision of about $100\,\mu$m: $75\,\mu$m for $B^0 \to f_{\rm CP}$ and $140\,\mu$m in a more complex case of $B^0 \to f_{\rm tag}$. These scales alone illustrate the level of difficulty of time-dependent measurements in a $B$ factory experiment.

The performance of vertexing and decay distances measurements in Belle is demonstrated by our measurement of $B$ mesons lifetimes. At a $B$ factory the decay distance in $z$ of a single $B$ meson can not be determined precisely because a position of the $B$ production point is not known accurately enough. All the tracks in the event belong to secondaries from both $B$'s decays, therefore the are no primary tracks left for the primary vertex determination. The beam spot position can not be used as the production point estimate because it is elongated too much: the size of the interaction region in $z$ direction amounts to $\sim 3$ mm.

Therefore, unlike the measurements at LEP or hadron machines, the lifetimes are determined from a distribution of the decay lengths difference $\Delta z$ of the two $B$ mesons, where one $B$ decay is fully reconstructed and only partial reconstruction is possible for the second $B$. It is in fact the same technique which is needed in the time-dependent CP asymmetries measurements. The measured lifetimes difference distributions for neutral and charged $B$ mesons are shown in Fig. 10. One sees a clear difference of widths of the distribution for the signal of the long lived $B$ decays and the distribution for backgrounds (dashed line) which measures our detector resolution. The fits to the distributions (solid line) yield precise determinations of the charged and neutral $B$ meson lifetimes [13] and their ratio: $\tau_+/\tau_0 = 1.09 \pm 0.03$ where the accuracy of the result, for the first time in a single measurement, allows the observation of the lifetimes difference. The detector resolution is understood over the span of 10 $B$ lifetimes and over 3 orders of magnitude in $B$ decay rate. This demonstrates our ability to measure time-dependent CP violation effects.

In the case of the CP asymmetry measurement the vertex position of the $B^0 \to f_{\rm CP}$ decay is determined using leptons from $J/\psi$ decays or charged hadrons from $\eta_c$ decays. The vertex of the $B^0 \to f_{\rm tag}$ is obtained using well reconstructed tracks that are not assigned to $f_{\rm CP}$. Each vertex position is required to be consistent with the interaction region profile, determined run-by-run, smeared in the $r$-$\phi$ plane to account for the $B$ meson decay length. With these requirements, we are able to determine a vertex even with a single track.

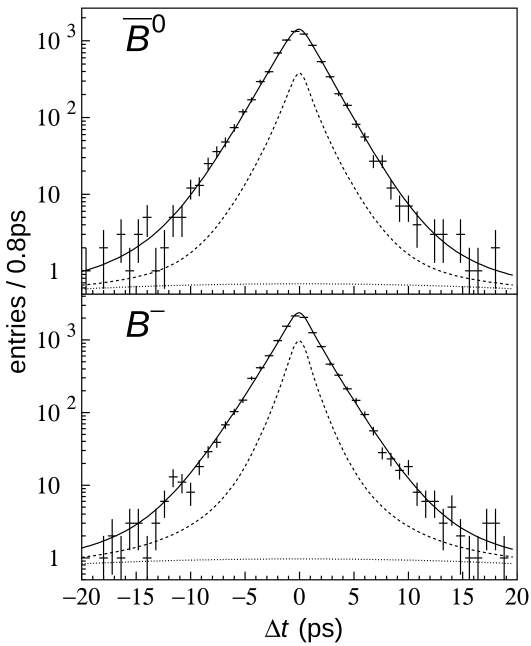


Fig. 10. The distribution of decay time differences between neutral $B$ mesons (top) and charged $B$ mesons (bottom) measured by Belle. The points are the data, the solid line is the result of a maximum likelihood fit that includes a component describing $B$ lifetime and two background components (dotted and dashed) that parametrise the detector resolution.

The $\Delta z$ resolution function is constructed by convolving four components: the detector resolutions, the shift in the tagging-side vertex position due to secondary tracks originating from charmed particle decays, and smearing due to the kinematic approximation used to convert $\Delta z$ to $\Delta t$ ($\Delta t = \Delta z/\beta\gamma c$). A small component of broad outliers in the $\Delta z$ distribution, caused by mis-reconstruction, is represented by a Gaussian function (like the one represented by dashed lines in Fig. 10). We determine twelve resolution parameters from fits of data to the neutral and charged $B$ meson lifetimes [13] and obtain an average $\Delta t$ resolution of $\sim 1.43$ ps (rms).

*4.4. Results and cross-checks*

Figure 11 shows the observed $\Delta t$ distributions for the $q\xi_{f_{\rm CP}} = +1$ (solid points) and $q\xi_{f_{\rm CP}} = -1$ (open points) event samples. The asymmetry between the two distributions shows clear indication of CP violation. We

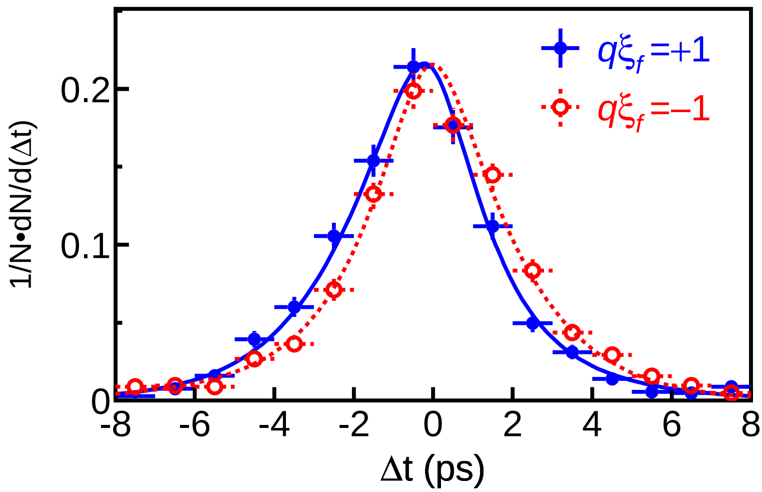


Fig. 11. The $\Delta t$ distributions measured by Belle: for the events with $q\xi_{f_{\rm CP}} = +1$ (solid points) and $q\xi_{f_{\rm CP}} = -1$ (open points). Solid and dashed lines show the results of the fit with $\sin 2\phi_1 = 0.72$.

determine $\sin 2\phi_1$ from an unbinned maximum-likelihood fit to the observed $\Delta t$ distributions. The probability density function (PDF) for the signal distribution is given by

$$P_{\rm sig}(\Delta t, q, w_l, \xi_{f_{\rm CP}}) = \frac{e^{-|\Delta t|/\tau_{B^0}}}{4\tau_{B^0}}[1 - q\xi_{f_{\rm CP}}(1-2w_l)\sin 2\phi_1 \sin(\Delta m_d \Delta t)] \,. \tag{20}$$

The $B^0$ lifetime $\tau_{B^0}$ and mass difference $\Delta m_d$ are fixed at their world average values [2]. The PDF is convolved with the appropriate $\Delta t$ resolution function to determine the likelihood for each event as a function of $\sin 2\phi_1$. The PDF for the combinatorial background is modelled as a sum of exponential and prompt components convolved with a sum of two Gaussians. The only free parameter of the fit is $\sin 2\phi_1$, and it is determined by maximising the likelihood function. The fit yields

$$\sin 2\phi_1 = 0.719 \pm 0.074({\rm stat}) \pm 0.035({\rm syst}) \,. \tag{21}$$

The systematic error is dominated by uncertainties in the vertex reconstruction (0.022). Other significant contributions come from uncertainties in $w_l$

(0.015), the resolution function parameters (0.014), a possible bias in the $\sin 2\phi_1$ fit (0.011), and the $J/\psi K_{\rm L}^0$ background fraction (0.010). The errors introduced by the uncertainties of $\Delta m_d$ and $\tau_{B^0}$ are less than 0.010.

Several checks of the result are performed. The analysis is repeated for various subsamples separately. The results are listed in Table IV; they are all consistent with each other. Figures 12(a)–(c) show the raw asymmetries and the fit results for all modes combined, for $(c\overline{c})K_{\rm S}^0$, and for $J/\psi K_{\rm L}^0$, respectively. A fit to the non-CP eigenstate modes $B^0 \to D^{(*)-}\pi^+$, $D^{*-}\rho^+$, $J/\psi K^{*0}(K^+\pi^-)$, and $D^{*-}\ell^+\nu$, where no asymmetry is expected, yields $0.005 \pm 0.015$(stat). Figure 12(d) shows the raw asymmetry for these non-CP control samples.

TABLE IV

The Belle meaurements of $\sin 2\phi_1$ for various subsamples (statistical errors only); $N_{ev}$: number of candidates in the subsample.

| Sample | $N_{\rm ev}$ | $\sin 2\phi_1$ |
|---|---|---|
| $J/\psi K_{\rm S}(\pi^+\pi^-)$ | 1116 | $0.73 \pm 0.10$ |
| other $(c\overline{c})K_{\rm S}$ modes | 523 | $0.67 \pm 0.17$ |
| $J/\psi K_{\rm L}$ | 1230 | $0.78 \pm 0.17$ |
| $J/\psi K*^0\ (K_{\rm S}\pi^0)$ | 89 | $0.04 \pm 0.63$ |
| $f_{\rm tag} = B^0\ (q = +1)$ | 1465 | $0.65 \pm 0.12$ |
| $f_{\rm tag} = \overline{B^0}\ (q = -1)$ | 1493 | $0.77 \pm 0.09$ |
| $0 < r \leq 0.5$ | 1600 | $1.27 \pm 0.36$ |
| $0.5 < r \leq 0.75$ | 658 | $0.62 \pm 0.15$ |
| $0.75 < r \leq 1$ | 700 | $0.72 \pm 0.09$ |
| data before 2001 | 1587 | $0.78 \pm 0.10$ |
| data in 2002 | 1371 | $0.65 \pm 0.11$ |
| All | 2958 | $0.72 \pm 0.07$ |

We assumed in the above fits $|\lambda| = 1$ which implies, as discussed in Section 2.4, no direct CP violation effects. This is the Standard Model expectation for the $B^0 \to c\bar{c}K^0$ decay. In order to test this assumption, we also performed a fit with $S_{f_{\rm CP}}$ and $|\lambda|$ as free parameters. We obtain

$$|\lambda| = 0.950 \pm 0.049(\text{stat}) \pm 0.025(\text{syst}) \tag{22}$$

and $-\xi_{f_{\rm CP}} S_{f_{\rm CP}} = 0.720 \pm 0.074$(stat) for all CP modes combined. This result is consistent with the assumption used in our analysis.

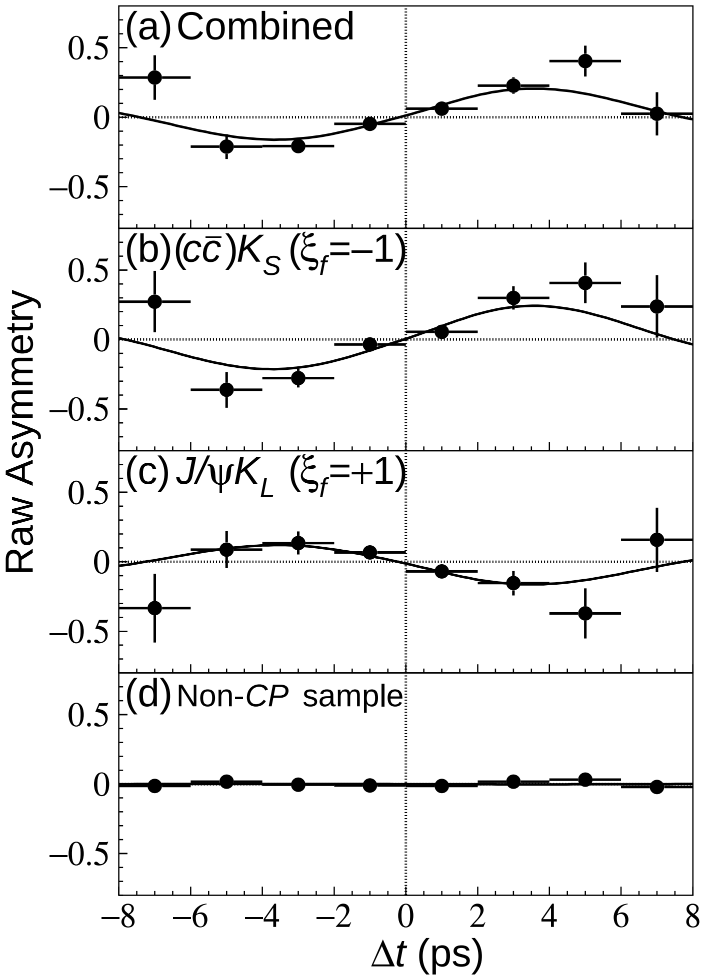


Fig. 12. The raw asymmetry in Belle data: (a) for all modes combined, (b) for $(c\bar{c})K^0_S$, (c)for $J/\psi K^0_{\rm L}$, and (d) for non-CP eigenstate control samples. The curves are the results of the unbinned maximum likelihood fit to the individual data samples.

BaBar finds [12] $\sin 2\phi_1 = 0.741 \pm 0.067 \pm 0.034$ for the data sample of comparable size to Belle's. The $\Delta t$ distributions and raw asymmetries measured by BaBar are shown in Fig. 13.

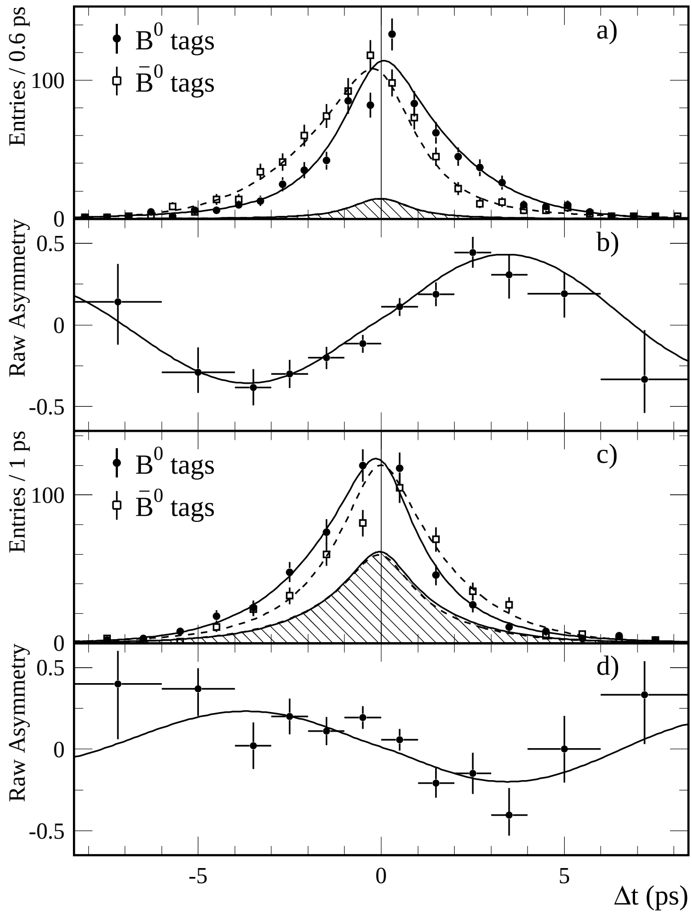


Fig. 13. BaBar data. The $\Delta t$ distributions and raw asymmetries: (a) and (b) for $\xi_f = -1$ candidates ($J/\psi K^0_{\rm S}, \psi(2S)K^0_{\rm S}, \chi_{c1}K^0_{\rm S}$ and $\eta_c K^0_{\rm S}$); (c) and (d) for $\xi_f = +1$ candidates ($J/\psi K^0_{\rm L}$). The shaded regions in (a) and (c) represent the background contributions, the solid(dashed) curves denote the fit projection for $B^0(\bar{B^0})$.

## 5. CP asymmetries in $B^0 \to \pi^+\pi^-$ decay

As discussed in Section 2.4, the decay $B^0 \to \pi^+\pi^-$ is a promising place to observe direct CP violating effects in $B^0\bar{B}^0$ oscillations. The two possible decay amplitudes, the tree and the penguin, in the decay path can give rise to appearance of a $\cos \Delta m_{B_d}\Delta t$ term in the asymmetry in addition to the sinus term. The measured $B^0 \to K^+\pi^-$ branching fraction, which is three times larger than the $B^0 \to \pi^+\pi^-$ branching fraction, suggests that the penguin amplitude is not small.

### 5.1. Selection of $B^0 \to \pi^+\pi^-$ candidates

The results presented here are from a data sample of $41.8\,\mathrm{fb}^{-1}$ collected by the Belle experiment. Details of the analysis can be found in Refs. [14,15].

The experimental technique is similar to that discussed at the $\sin 2\phi_1$ measurement, there are however a number of complications. The vertexing and flavour tagging described in Sections 4.2 and 4.3 applies the same to the $\pi^+\pi^-$ asymmetry measurement, however the candidates selection is more challenging. The branching fraction for $B^0 \to \pi^+\pi^-$ is quite small compared to the charmonium modes, only $(4.8 \pm 0.6) \times 10^{-6}$. Furthermore the two-body decay results in high momentum tracks, making these candidates look more like $e^+e^- \to q\bar{q}$ continuum background, thus more efficient background suppression is needed. For this purpose we use a Fisher discriminant determined from event shape variables (Fox–Wolfram moments) and the reconstructed $B^0$ direction in the cms with respect to the beam axis. Fig. 14 shows the distribution of the background suppression variable (Likelihood Ratio LR) for the signal events (open circles) and off-resonance data (closed circles). By requiring LR $> 0.825$ the continuum background is reduced by

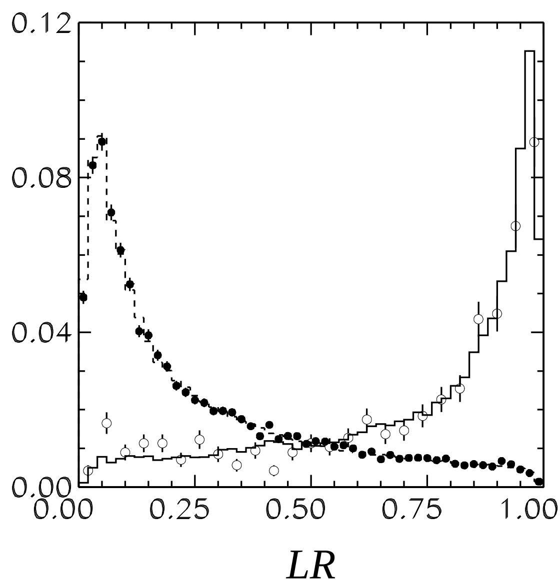


Fig. 14. The distribution of background suppressing variable LR: solid points are continuum data, the open points: the signal (control sample of fully reconstructed low multiplicity $B$ decay channels). $B^0 \to \pi^+\pi^-$ candidates are selected with LR $> 0.825$.

an order of magnitude, while retaining two third of the signal. The strong background from $B^0 \to K^+\pi^-$ decay is suppressed by using kaon identification. Figure 15 shows the $\Delta E$ distribution for $\pi^+\pi^-$ candidates. The signal yield is extracted by fitting the $\Delta E$ distribution with a Gaussian $\pi^+\pi^-$ signal function, plus contributions from misidentified $B^0 \to K^+\pi^-$ events, three-body $B$-decays, and continuum background. From the fit, we estimate the numbers of events: $73.5 \pm 13.8$ $\pi^+\pi^-$ events, $28.4 \pm 12.5$ $K^+\pi^-$ events, and $98.7 \pm 7.0$ continuum events in the signal region. The $K^+\pi^-$ contamination is consistent with the $K \to \pi$ misidentification probability measured independently. The contribution from three-body $B$-decays is negligible in the signal region.

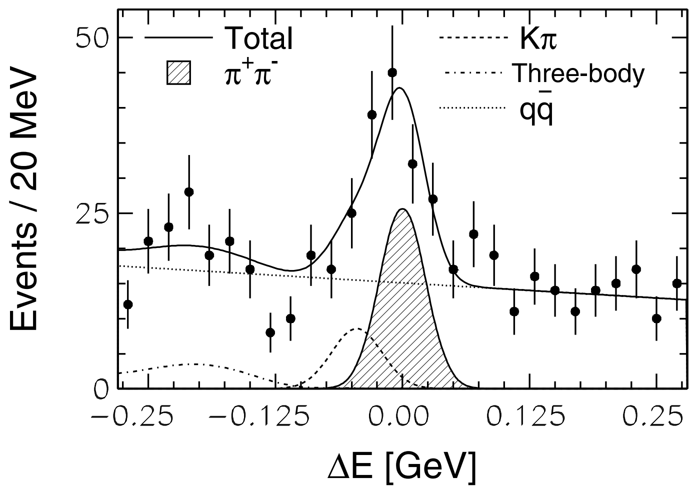


Fig. 15. The energy difference distribution $\Delta E$ for the $B^0 \to \pi^+\pi^-$ candidates. The signal peaks at $\Delta E = 0$ (hatched Gaussian), the remaining $K^+\pi^-$ background peaks at $-0.045$ (dashed Gaussian). The continuum is parametrised as a falling background, while $B^0$ decays with $> 2$ particles in the final state appear at low negative $\Delta E$.

### *5.2. Time dependent asymmetry*

The $\Delta t$ resolution for the signal is parametrised by convolving a sum of two Gaussians with a function that takes into account the cms motion of the $B$ mesons. The resolution function for the background has the same functional form but the parameters are obtained from a sideband region in $m_{bc}$ and $\Delta E$. Using these resolution functions, we determine a $B^0$ lifetime for the $B^0 \to \pi^+\pi^-$ candidates. The fit yields $\tau_{B^0} = 1.49 \pm 0.21(\text{stat})$ ps, which is consistent with the world average [2].

After flavour tagging and vertexing requirements are applied, an unbinned maximum-likelihood fit to the $\Delta t$ distributions is performed with the two CP violation parameters as the only free parameters. For the calculation of the PDF, the purity of events is determined event-by-event in a function of $\Delta E$ and $m_{\rm bc}$, properly normalised by the average signal and background fractions in the signal region.

The result of the fit to the 162 candidates (92 $B^0$- and 70 $\overline{B^0}$-tags) that remain after flavour tagging and vertex reconstruction is:

$$\begin{aligned} S_{\pi\pi} &= -1.21^{+0.38}_{-0.27}(\text{stat})^{+0.16}_{-0.13}(\text{syst})\,; \\ A_{\pi\pi} &= +0.94^{+0.25}_{-0.31}(\text{stat}) \pm 0.09(\text{syst})\,. \end{aligned}$$

The result is $1.3\sigma$ away from the physical boundary $S^2_{\pi\pi} + A^2_{\pi\pi} = 1$, which is still consistent with a statistical fluctuation. Each of these two measurements is less than $3\sigma$ away from zero, which is not yet statistically significant. The correlation between $S_{\pi\pi}$ and $A_{\pi\pi}$ is 0.28. More details can be found in Ref. [14].

The $\Delta t$ distributions before and after background subtractions together with the fit results (solid lines) are shown in Fig. 16.

We have performed a number of cross-checks of these results, including fits to $B^0 \to K^+\pi^-$ which should not exhibit any CP asymmetry or fits to the background from side-bands (Fig. 16 (e)). None of this fits show significant asymmetry.

BaBar results on the $B^0 \to \pi^+\pi^-$ are based on a sample of $88 \times 10^6 B\bar{B}$ pairs. Their methodology differs from Belle's. They perform a multidimensional fit to a sample of 26070 events of which $157 \pm 19 \pm 17$ are signal events. The fit has a total of 76 parameters, among them the CP violation parameters $S_{\pi\pi}$ and $A_{\pi\pi}$. The observed flavour tagged $\Delta t$ and asymmetry distributions in BaBar data, after applying cuts to enhance the signal fraction, are shown in Fig.17. In contrast to Belle, BaBar obtains:

$$\begin{aligned} S_{\pi\pi} &= +0.02 \pm 0.34 \pm 0.05\,, \\ A_{\pi\pi} &= +0.30 \pm 0.25 \pm 0.04\,. \end{aligned}$$

The $S_{\pi\pi}$ results of the two experiments are statistically marginally consistent.

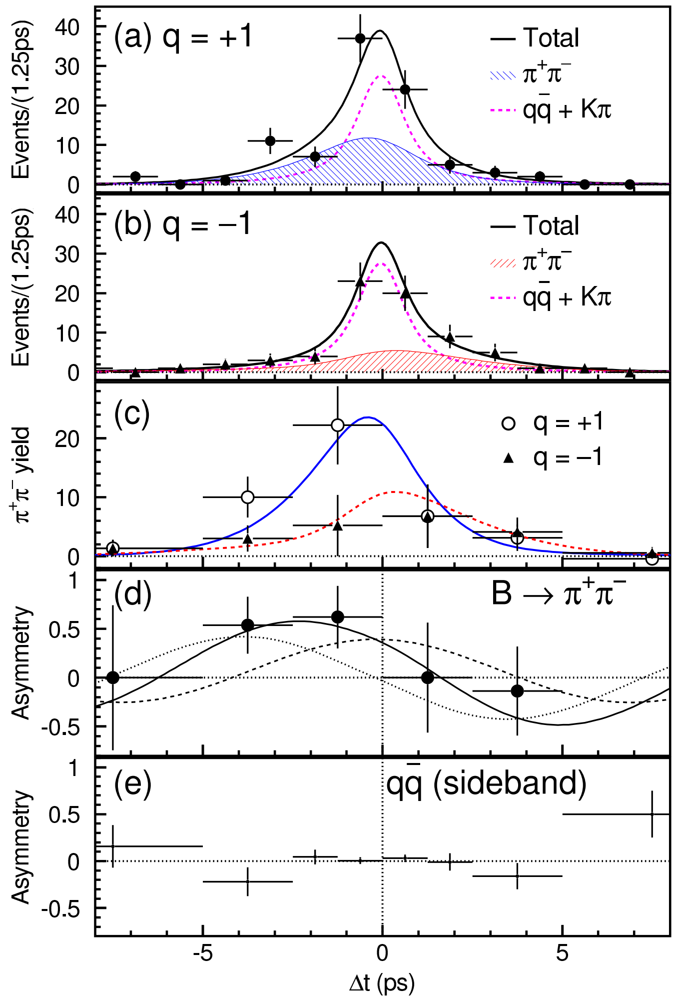


Fig. 16. The $\Delta t$ and asymmetry distributions for the $B^0 \to \pi^+\pi^-$ candidates in Belle data. (a) $f_{tag} = B^0$ candidates ($q = +1$); (b) $f_{tag} = \bar{B}^0$ candidates ($q = -1$); (c) $\pi^+\pi^-$ yields after background subtraction. The errors are statistical only. (d) the CP asymmetry for $B^0 \to \pi^+\pi^-$ after background subtraction. (e) the raw asymmetry for $B^0 \to \pi^+\pi^-$ sideband (background) events. The curves in (a)–(c) show the results of the unbinned maximum likelihood fit. The solid curve in (d) shows the resultant CP asymmetry, the dashed (dotted) curve denotes the contribution from the cosine (sine) term.

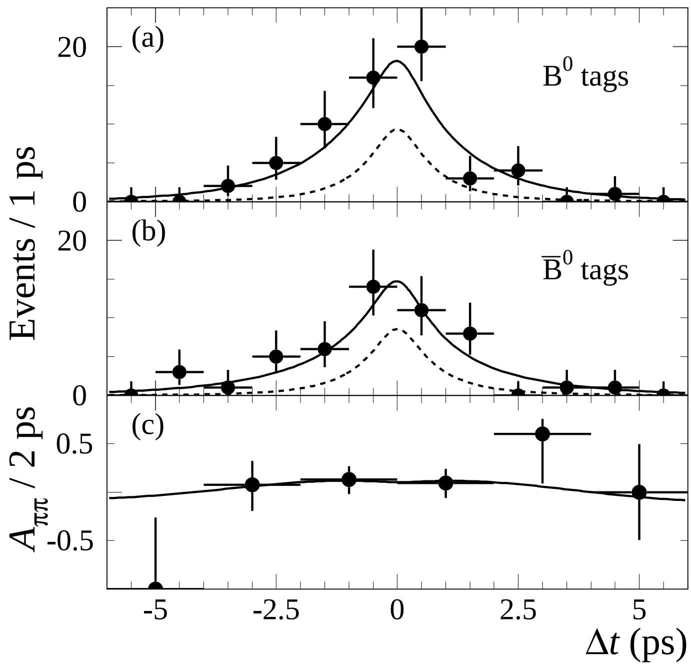


Fig. 17. BaBar data. The $\Delta t$ and asymmetry distributions for the $B^0 \to \pi^+\pi^-$ candidates: $\Delta t$ for (a) $B^0$ tags and (b)$\bar{B^0}$ tags; (c) the asymmetry $A_{\pi\pi}(\Delta t)$. The solid curves represent the projections of the unbinned maximum likelihood fit, dashed curves represent background distributions.

## 6. Summary and future prospects

The primary milestone of the $B$ factories, a precise measurement of $\sin 2\phi_1$, has been achieved in less than four years of their operation. CP violation in the $B^0$ meson system has been unambiguously established: the combined result of BaBar and Belle measurements, $\sin 2\phi_1 = 0.731 \pm 0.055$, has an accuracy better than 10%. This result is consistent with indirect determinations based on the Standard Model consistency fits that use the measurements sensitive to the sides of the unitarity triangle, the measurement of $\epsilon_K$ and several phenomenological inputs. This agreement strongly suggest that the Kobayashi–Maskawa ansatz is very likely the dominant source of CP violation in flavour changing processes.

The $\sin 2\phi_1$ measurement is the first step in over-constraining the KM model of CP violation. There are many promising rare $B$ decay modes which are much more sensitive to new physics effects than the golden decay mode $J/\psi K$. First interesting measurements of CP asymmetries started to emerge, like these for $B \to \pi\pi$ (or not discussed here $B \to \phi K$, $\eta' K$). They are still statistically limited, but some of them will become significant soon with larger data samples. Data samples of each experiment will triple in less than three years, with the present performance of the $B$ factories. Moreover, both experiments have plans for their machines and detectors upgrades in 2006. $B$ super-factories with luminosities exceeding $10^{35}\mathrm{cm}^{-2}\mathrm{s}^{-1}$ are planned, to accumulate at least $10^3\mathrm{fb}^{-1}$ of data — a tenfold of the present statistics.

I wish to acknowledge the essential contributions of my colleagues in Belle and BaBar to the results described here. I also thank the organizers of the School for their kind invitation and hospitality. This work was partially supported by the Polish State Committee for Scientific Research (KBN) under grant no. 2P03B17017.

## REFERENCES

[1] M. Kobayashi, T. Maskawa, *Prog. Theor. Phys.* **49**, 652 (1973).

[2] K. Hagiwara *et al.* (Particle Data Group), *Phys. Rev.* **D66**, 010001 (2002).

[3] L. Wolfenstein, *Phys. Rev. Lett.* **49**, 1945 (1983).

[4] I. Bigi et al., in *CP Violation*, C. Jarlskog ed., World Scientific, Singapore 1988.

[5] A.B. Carter, A.I. Sanda, *Phys. Rev.* **D23**, 1567 (1981); I.I. Bigi, A.I. Sanda, *Nucl. Phys.* **B193**, 85 (1981).

[6] P. Oddone, in *Proceedings of the UCLA Workshop: Linear Collider $B^0\bar{B}^0$ Factory Conceptual Design*, edited by D. Stork, World Scientific, 1987, p. 243.

[7] B. Aubert *et al.*, (Belle Coll.), *Nucl. Instrum. Methods Phys. Res.* **A479**, 1 (2002).

[8] A. Abashian *et al.*, (Belle Coll.), *Nucl. Instrum. Methods Phys. Res.* **A479**, 117 (2002).

[9] KEK Report No. 2001-157, edited by E. Kikutani, 2001, to be published in *Nucl. Instrum. Methods Phys. Res. A*.

[10] K. Abe *et al.* (Belle Coll.), *Phys. Lett.* **B538**, 11 (2002).

[11] K. Abe *et al.* (Belle Coll.), *Phys. Rev. Lett.* **87**, 091802 (2001); K. Abe *et al.* (Belle Coll.), `hep-ex/0202027` (to be published).

[12] B. Aubert *et al.* (BaBar Coll.), `hep-ex/0207042`, submitted to *Phys. Rev. D*.

[13] K. Abe *et al.* (Belle Coll.), *Phys. Rev. Lett.* **88**, 171801 (2002).

[14] K. Abe *et al.* (Belle Coll.), *Phys. Rev. Lett.* **89**, 071801 (2002).

[15] K. Abe *et al.* (Belle Collab.), *Phys. Rev. Lett.* **87**, 101801 (2001); Paper is in preparation, to be submitted to *Phys. Rev. D*.

[16] B. Aubert *et al.* (BaBar Coll.), `hep-ex/020755`; B. Aubert *et al.* (BaBar Coll.), *Phys. Rev.* **D65**, 051502 (2002).